Electrons scattered inside small dust grains of various materials

Ivana Richterová, Martin Beránek, Jiří Pavlů,* Zdeněk Němeček, and Jana Šafránková
Faculty of Mathematics and Physics, Charles University, Prague, Czech Republic
(Received 25 September 2009; published 4 February 2010)

The dust grain charge in an electron beam is given by a difference in numbers of electrons that fall onto the grain and those leaving it. Electrons with energies exceeding 1 keV can penetrate through submicron-sized dust grains. If the grain is small enough, a yield of these electrons reaches unity but they leave a part of their energy inside the grain and this energy excites secondary electrons. The paper presents a hybrid Monte Carlo code that simulates paths of the primary electrons inside a spherical grain and provides the yield of scattered electrons and their energy spectrum as a function of the grain size and material. This code is based on the Richterová *et al.* [Phys. Rev. B **74**, 235430 (2006)] model but it includes several corrections important for light materials like carbon or ice. The model was verified using experimental results obtained on large planar samples. For spherical samples, we have found that the yield of scattered electrons reaches unity for 50 nm Au grains illuminated by 5 keV electrons, whereas the same effect can be observed on ≈1000 nm carbon grains.

DOI: 10.1103/PhysRevB.81.075406 PACS number(s): 79.20.Hx, 94.05.Bf, 52.27.Lw

I. INTRODUCTION

Dust grains immersed in a plasma environment interact with surrounding ions and electrons. If the electrons are energetic enough, they can be scattered and/or release low-energy secondary electrons. Secondary electron yield is a ratio of impinging electrons to true secondary electrons, while the scattered electron yield gives a relative number of scattered electrons. The latter will be widely discussed in the present paper; thus, we will call it simply "yield" hereafter. Note that scattered electrons are often called backscattered electrons or, in the case of thin films, they can be separated into two groups: forward-scattered and backscattered electrons. Due to a geometry of our approach, we do not distinguish between forward-scattering and backscattering; thus, we use the term "scattered electrons." Photoemission as well as ion impacts cause a positive charging current, while a total secondary electron yield can be smaller or larger than unity. Although different kinds of emissions were studied in detail for bulk samples, conclusions should be used carefully for the dust grains of sizes comparable with a penetration depth of primary particles.

The principal difference between experiments with planar samples and dust grains immersed in the plasma environment is their charging. Whereas the potential of large targets is usually well defined, the dust grain potential is set self-consistently to achieve a zero net charging current. However, various constituents of the charging current respond to the grain potential by different ways. Whereas photons are not affected by the grain potential, the number of photoelectrons leaving the grain decreases if the grain potential becomes more positive. The interaction of electrons and ions with the grains of a given potential is comprehensively discussed for example in Meyer-Vernet,[2] de Angelis,[3] and Goertz;[4] thus, we mention only a basic mechanisms.

For the negative charged grain, the number and energy of impinging ions increase and thus the number of electrons emitted by the ion impact increases. On the other hand, primary electrons if they are energetic enough are decelerated and deflected. Their effect on the secondary electron production depends on the relative speed between primary electrons and the dust grain and their number can increase as well as decrease with the grain surface potential. This complicated behavior results in the fact that for sufficiently high values of the secondary yield the current balance equation can have more than one solution for the equilibrium potential.[4]

Published experimental values of secondary emission yields measured on large planar samples of various materials can differ by a factor of 2, probably due to different conditions and sample quality. The excellent set of these data measured under 10^{-7}–10^{-9} Torr has been collected by Bronstein and Fraiman,[5] and recently it was revised by El Gomati *et al.*[6] and Walker *et al.*[7] for both scattered and secondary yields, respectively. Their papers also deal with the influence of surface adsorbates and oxide layers on the secondary yield. Unfortunately, the surface coarseness was not reported.

During the past several years, an enhanced attention has been directed toward electron interaction with solid planes and films and its numerical simulations. This interest arises from applications of scanning electron microscopy to the analysis of conductors as well as non- or poorly conducting materials such as polymers, ceramics, biological material, and composites.

In widely used Monte Carlo simulations, two phenomena should be modeled: elastic collisions and energy losses. Inelastic collisions are usually neglected due to a small deflection angle[8] resulting from such events and they are considered to be continuously distributed along the paths of primary electrons. A slowing-down equation based on the stopping-power Bethe expression[9] usually simulates these energy losses. However, in the low-energy range, this expression must be reevaluated since the number of possible inelastic events is decreasing.[10]

For elastic events, the Rutherford theory[11] has been widely applied due to its simplicity and its short computation time.[12] This model is accurate for a high-energy interaction (>10 keV) because it is based on the first Born approximation. However, a more accurate Mott theory[13] is preferable at lower energies. Empirical forms of the Mott cross–sections have been developed recently (e.g., Browning[14]). The differential Mott cross sections for a number of elements of the

periodic table were computed by Czyżewski *et al.*[15]

On the other hand, electron emission from micron- and submicron-sized grains was studied by several authors only; for example, Draine and Salpeter[16] estimated enhancement of a secondary yield due to finite grain size; Ziemann *et al.*[17] observed the accumulated charge on small oil drops falling through an electron beam; while Švestka *et al.*[18] started a series of measurements of an equilibrium surface potential of single isolated dust grains. Pavlů *et al.*[19] found that the equilibrium surface potential is growing with the energy above ≈2 keV for micron-sized glass grains. The authors observed that the surface potential of large gold grains reaches a maximum of about 15 V at 1.2 keV and drops to 5 V at 10 keV. By contrast, a 0.6 μm gold grain exposed to an electron beam of energy 10 keV charges to 7 V, while the 0.3 μm grain to 17 V.

To explain laboratory experiments, several numerical models of electron-matter interactions inside dust grains were developed. Ziemann *et al.*[17] reported a mechanism for an increasing secondary electron yield with a decreasing oil drop size. Chow *et al.*[20] proposed an analytical model that attributed the mentioned enhancement of the grain potential to the increase of the yield of true secondary electrons. However, the modeled results did not fit the experimental data of Švestka *et al.*[18] in the full energy range. Richterová *et al.*[1,21] developed a hybrid Monte Carlo model. The model shows that the increase of the grain potential occurs for grain sizes comparable to a penetration depth of primary electrons and that it is caused by a larger portion of primary electrons being scattered out of the grain. The corresponding increase of the secondary yield is rather tiny and has a minor effect on the resulting potential. This model was successfully verified by laboratory experiments dealing with charging of gold[1] and glass[22] dust grains. However, further investigations revealed a few differences between model predictions and experiments for some light species such as carbon. The present paper analyzes sources of these differences and suggests appropriate corrections. The corrected model is then used for calculations of the scattered yield and energy spectra of scattered electrons. To present the model results, we compare different materials and diameters of grains starting from 50 nm.

II. PHYSICAL BACKGROUND OF THE MODEL

The basic model is described in Richterová *et al.*;[1] thus, this paragraph summarizes only briefly basic principles and the following paragraphs are devoted to a description of suggested model corrections. The model is based on the Hovington *et al.*[23] approach. The grain material is defined by its mass density and elemental composition. The model is three-dimensional (3D) and can deal with grains of arbitrary shapes and even simulate the dust grains consisting of several material regions as various layers or small features embedded inside the grain. A path of primary electrons is computed individually inside a continuous matter, i.e., crystal lattice effects are ignored. The electrons are traced until being scattered out of the grain or slowed down to 20 eV. The grain is bombarded by a parallel electron beam of the energy, E. The beam (primary) electrons undergo both elastic and inelastic collisions inside the grain. Since a deflection of a primary electron in inelastic collisions is small, they are replaced by continuous energy losses along its path between two consecutive elastic collisions. Elastic collisions change the electron direction randomly in accord with the differential cross section.

A path traveled between two subsequent elastic collisions and a deflection angle are generated according to energy-dependent Mott's atomic radial cross section.[13] Note that the supplemental polar angle is generated randomly. We use values of cross sections computed by Czyżewski *et al.*[15] through a relativistic Hartree-Fock-Slater potential. These values are a bit overestimated what compensates the omitted deflections by inelastic collisions.[15] Since the cross sections are published as a table, we are using a linear interpolation for intermediate values. In the case of compounds, we do not compute a weighted differential cross section but a random number is generated to decide which of particular species causes the electron deflection at each collision.

Integrating the radial cross section over a whole space angle, we can obtain a total cross section, $\sigma_T(E)$. σ_T decreases monotonously with the energy and can be well interpolated via cubic splines.

The mean-free forceless path, λ, can be expressed as

$$\lambda(E) = \left[\sum n_j \sigma_{Tj}(E)\right]^{-1}, \tag{1}$$

where n_j is a number density of deflecting atoms of jth elemental species. A path between two subsequent collisions can be written as $-\lambda(E)\ln(\xi)$, where ξ is a uniform random number. Expression (1) was used in Richterová *et al.*,[1] but it neglects changes of the electron energy between two elastic collisions.

Since the electron energy decreases (and σ_T increases) along its path, electrons travel a shorter path between subsequent collisions than that given by mean-free path (1). The probability, P that an electron of the energy E does not undergo any collision decreases with the path length, Δs exponentially,

$$P(E,\Delta s) = \exp[-f(E,\Delta s)]. \tag{2}$$

The accumulation function, $f(E,\Delta s)$ can be written as

$$f(E,\Delta s) = \int_{s(E)}^{s(E)+\Delta s} \sum n_j \sigma_{Tj}(s')ds'. \tag{3}$$

This equation simplifies to Eq. (1) if the deceleration is omitted. If not, generating the path segment between two subsequent collisions requires solving an expression,

$$f(E,\Delta s) = -\ln(\xi).$$

As noted above, all inelastic events are simulated by the stopping power. Richterová *et al.*[1] used well-established modified Bethe stopping power formula[12]

$$\frac{dE}{ds} \sim -\frac{\varrho}{N}\frac{A}{E}\ln\frac{1.166(E+0.85J)}{J}, \tag{4}$$

where E is an actual electron energy, s is a traveled path, ϱ is a mass density, A and N are atomic and nucleon numbers,

TABLE I. Material constants used in calculations: atomic number (A), nucleon number (N), mass density (ϱ), and mean ionization potential (J). The values are adopted from Berger and Seltzer[24] except the mass density of glassy carbon; a value for graphite is used here.

Matter	A	N	ϱ (g cm^{-3})	J (eV)
Ice	3.33	6.0	0.92	75.0
g-carbon	6	12.0	1.54	78.0
Glass	10	20.0	2.20	139.2
Aluminum	13	27.0	2.70	166.0
Copper	29	63.5	8.93	322.0
Gold	79	197	19.3	790.0

and J is a mean ionization potential. The first term is proportional to the atom density that, multiplied by A, corresponds to the total density of electrons. $1/E$ is proportional to probability of an inelastic collision, and the last term represents a mean transferred energy. A, N, and J can be determined for compounds from their stoichiometric indices. Material constants collected by Berger and Seltzer[24] used for calculations in the next section are summarized in Table I.

The term $0.85J$ in Eq. (4) ensures that the stopping power drops but does not change sign at the lowest energies. This approach is quite rough and worthwhile only down to energies of $0.15J$, i.e., to $\approx$10 eV for carbon or glass but to $\approx$100 eV for gold or silver. More realistic and accurate results can be achieved if the stopping power is calculated omitting inner electron shells that cannot participate in inelastic collisions at the lowest energies. Then, Eq. (4) can be rewritten as

$$\frac{dE}{ds} \sim -\frac{\varrho}{N}\frac{A_{\mathrm{eff}}(E)}{E}\ln\frac{1.166E}{J_{\mathrm{eff}}(E)}. \tag{5}$$

The effective number of atom electrons, $A_{\mathrm{eff}}(E)$ and the effective mean ionization potential, $J_{\mathrm{eff}}(E)$ can be derived from the energy-loss function that represents a dielectric response of material to a passage of charged particles[25] or electromagnetic radiation (for details see Refs. 8, 10, and 23).

The selected stopping power is preprocessed together with Mott's total cross sections as follows:

(i) the traveled path as a function of the electron energy, $s(E)$ is calculated from Eq. (4) and (5);

(ii) the resulting path, $s(E)$ is used to calculate the accumulation function, $f(E,s)$ that can be interpreted as a mean number of collisions; and

(iii) finally, having a uniform random number ξ, we compute the electron energy at $(k+1)$-th collision solving $f(E_{k+1})-f(E_k)=-\ln(\xi)$ and hence $\Delta s=s(E_{k+1})-s(E_k)$.

Both functions $s(E)$ and $f(E)$ are precalculated down to 20 eV with a logarithmic step having 100 points per decade, i.e., the step is $\approx$300 eV at 10 keV and $\approx$0.5 eV at 20 eV. It was verified that the step scaling of precalculated values is sufficient for the linear approximation.

III. RESULTS AND DISCUSSION

Since experimental values of scattered yields from curved samples are not available, we compare the model results with data measured on planar samples. The calculations were made under an assumption of the grounded target (no charging was expected) to be consistent with the conditions of experiments. Figure 1(a) shows that the Richterová *et al.*[1] and present model corrections differ predominantly for light species and thus the results for carbon are shown. The dashed line presents the scattered yield, η as a function of the primary energy as calculated by Richterová *et al.*,[1] whereas the full line stands for the results of the present model. Different symbols show the experimental data already published (see the figure caption for the sources). Unfortunately, as we already pointed out, the experimental data differ by a factor of 2, especially at low primary energies where the difference between two models is largest. Moreover, there is a lack of the experimental data below 200 eV. Nevertheless, we can conclude that the calculations are more realistic because they fall well among the measured points. We have made a similar comparison for other species and

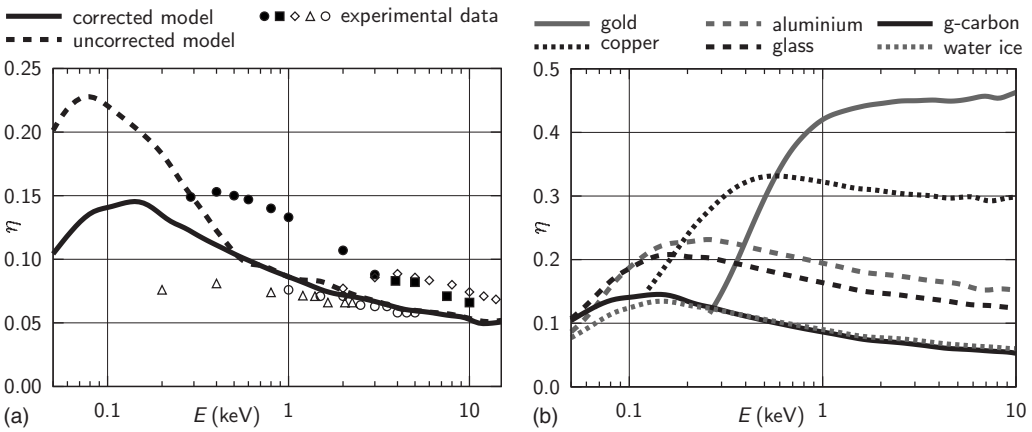

FIG. 1. Influence of a slowing-down correction and a total elastic cross-section sampling on profiles of the modeled scattered yields, η for a normal angle of incidence and for (a) glassy carbon, and (b) other planar materials. Experimental points: ●, Bronstein and Fraiman (Ref. 5); ■, Hunger and Küchler (Ref. 26); ◇, Palluel (Ref. 27); △, Sternglass (Ref. 28); ○, Assad and El Gomati (Ref. 29).

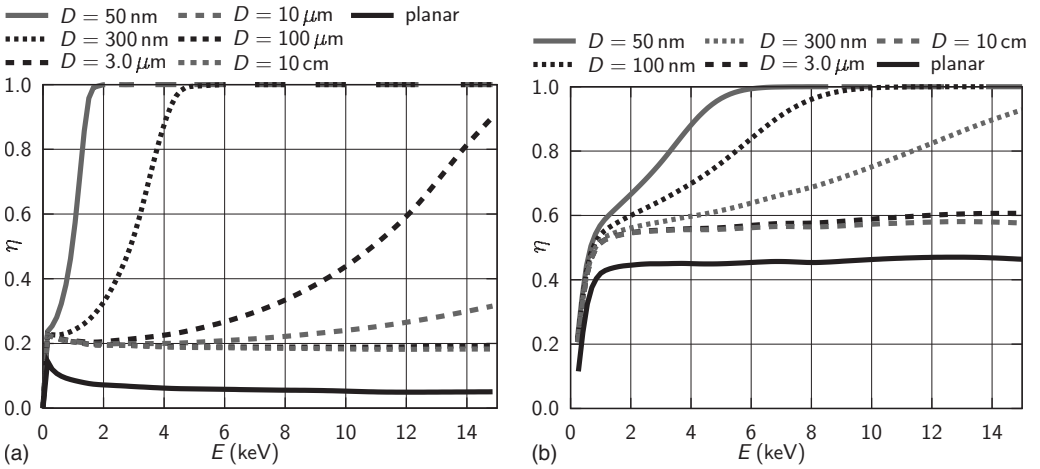

FIG. 2. Variations in modeled scattered yield profiles with the grain sizes and their comparison with a planar sample for (a) glassy carbon and (b) gold grains.

found that our simulated values seem to be a little lower than experimental data for very light species. It is probably a result of omission of the inelastic scattering that is more effective for these species. Czyżewski *et al.*[15] suggested to multiply the Mott cross section by a factor $(A+1)/A$ to account for this effect. We have checked this suggestion but the change was well within the spread of the experimental data. For this reason, the calculations presented further follow the described procedure and aforementioned correction is not implemented.

Figure 1(b) shows the results for planar samples of different materials. As it can be seen from the figure, the scattered yield is roughly constant above 2 keV of the primary energy and increases with the mean atomic number of the target.

Scattered yields as a function of the energy and grain size are plotted in Fig. 2. The calculations for planar samples are shown as a reference. The difference between planar and large spherical samples is caused by the varying incidence angle along the spherical surface. It is interesting to note that the scattered yield increase due to the surface curvature is approximately the same for all investigated materials and it is equal to ≈0.13 for the energies above 2 keV. This means that a relative effect of the surface curvature decreases with an increasing atomic number.

Another interesting difference between spherical and planar samples is presence of overshoots of the energetic profiles of the scattered yield at low energies that are observed for all materials except gold in Fig. 2. These overshoots are observed for planar surfaces but they vanish for spheres of any diameter. We have no clear explanation for this effect but we think that it is a reason why the calculations of the dust grain charge using the original Richterová *et al.*[1] model were in a good agreement with experiments,[1,22] although this overshoot is strongly overestimated in this model (Fig. 1). The growth of the yield toward unity was found for spherical grains of all materials. A comparison of the panels of Fig. 2 shows that the yield growth depends on both the grain size and material. For example, a 100 nm gold grain behaves in a similar way as a 1 μm ice grain.

For better understanding of presented trends, several survey plots are discussed in following paragraphs. As it can be seen in Fig. 2, the backscattered yield, η is roughly constant above 2 keV of the primary energy for large spheres. This yield as a function of the atomic number is plotted in Fig. 3(a) [the points stand for the yields at 7 keV of the primary energy and materials from Fig. 1(b)]. The scattered yield grows with the atomic number as $\ln(A^{0.15})$ what is in a good agreement with previous measurements.[5] The points in the

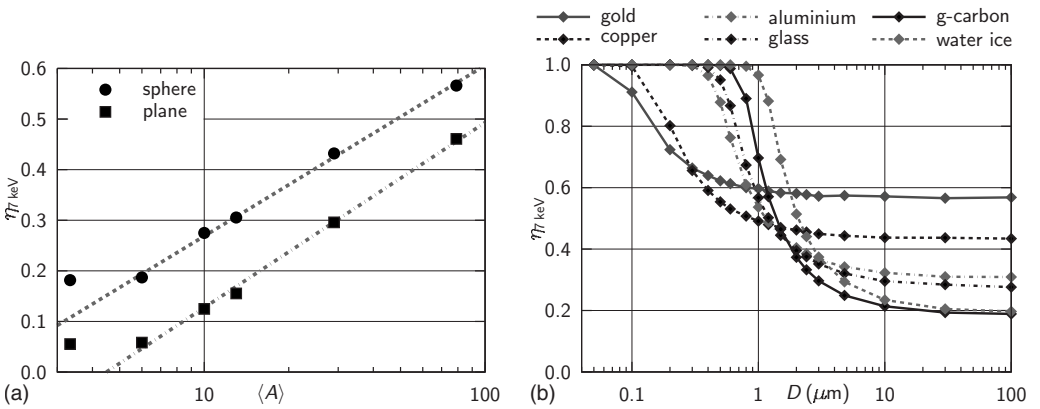

FIG. 3. (a) Scattered yields for the 7 keV primary energy as a function of the atomic number. The yield grows as $\ln(0.93\times A^{0.15})$ and $\ln(0.79\times A^{0.16})$ for large spheres and plates, respectively. (b) Calculated scattered yields as a function of the grain diameter, D for various materials at the beam energy of 7 keV.

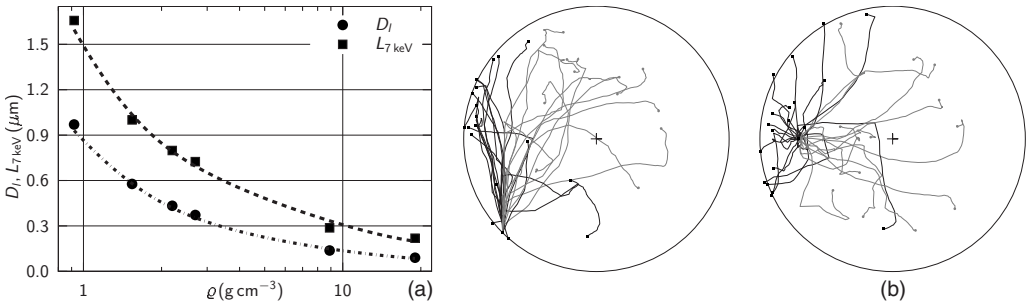

FIG. 4. (a) A limit diameter (D_l) and total path length (L) of 7 keV electrons (calculated from Eq. (4)) as a function of the mass density. (b) A planar projection of several 7 keV electrons traced inside the 0.6 μm(=L) glassy carbon spherical grain; the planes perpendicular (left) and parallel (right) containing the grain to the beam direction are shown (the angle of incidence 45° was chosen). The black trajectories correspond to the scattered electrons, while the gray color marks the electrons captured inside a grain.

left bottom corner were calculated for ice and we would like to note that the relative atomic number of 6 would describe its properties better than the value of 3.33 given by its stoichiometry. This feature can be ascribed to much larger (by a factor of 10) deflection by oxygen atoms in comparison with hydrogen atoms.

The scattered yields of various materials as a function of the grain size, D for one primary energy (7 keV) are plotted in Fig. 3(b). One can see that η is constant for large grains and starts to change for about micron-sized grains. The general trend can be written as

$$[\eta(D) - \eta_{\text{inf}}]/(1 - \eta_{\text{inf}}) = (D/D_l)^{-1.17},$$

where D is the grain size, D_l is the limit grain size: $\eta(D_l)=1$, and η_{inf} stands for the scattered yield of a large grain of the infinite diameter (10 cm grain is a good approximation). The model predicts a slower growth of η than that of Chow *et al.*[20] Using a deflectionless movement of electrons, they obtained $\eta=(D/L)^{-2}$ where L is the total path length of electrons traveled in the matter before being thermalized.

While η of large samples is given by matter ability to deflect electrons, D_l and L are related to the mass that electrons have to pass through the grain material. In order to show it more clearly, D_l and L are plotted as a function of the mass density in Fig. 4(a). Both quantities decrease smoothly by a similar way but there is not a linear relation; D_l/L decreases from 0.6 for carbon to 0.4 for gold. In other words, when the total electron path length is equal to a grain diameter, not all electrons are capable to leave the grain.

An example of such wandering trajectories for a glassy carbon grain is given in Fig. 4(b) where several electron trajectories are projected onto two perpendicular planes. The electrons enter the grain at one point and they are scattered through the whole grain volume. The primary energy of 7 keV corresponds to L equal to the grain diameter. The colors distinguish captured (gray) and scattered (black) electrons. One can clearly see that only about a half of the electrons is scattered out of the grain.

The resulting spectra of electrons leaving a sample provide a supplementary information about the electron-matter interaction. Figure 5 shows the spectra of 10 keV electrons for gold and glassy carbon plates and grains of different diameters. For the gold plate [Fig. 5(a)], we obtained a spectrum with the characteristic peak near to the primary energy. The spectrum is in a good agreement with experimental results and with the model of Ding *et al.*[30] A small difference in the low-energy range is caused by the methodology. We have traced only primary electrons, whereas cascaded secondary electrons contribute to the energy spectrum in experi-

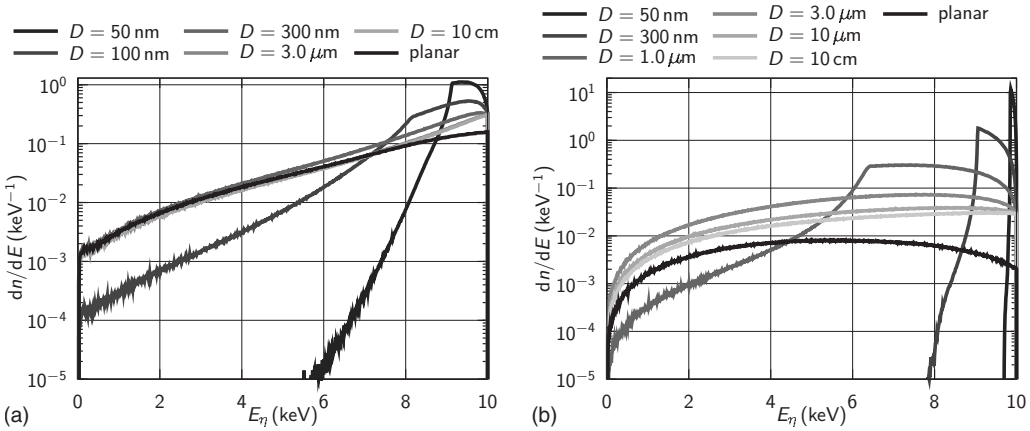

FIG. 5. Calculated spectra of 10 keV electrons scattered from grains of various sizes and from the plate for gold (a) and glassy carbon (b) grains.

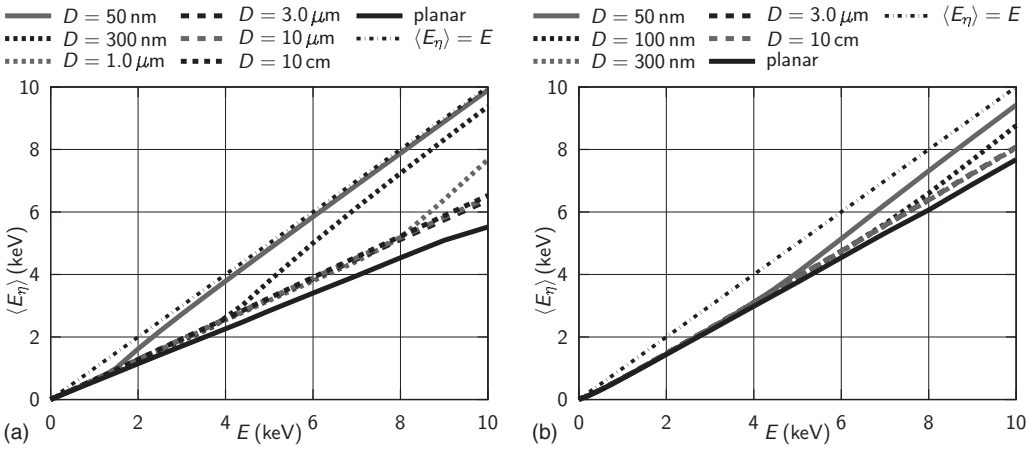

FIG. 6. A mean energy of scattered electrons as a function of the beam energy and the grain size for glassy carbon (a) and gold (b) grains. Slopes are 0.56 (plate) and 0.63 (large spheres) for glassy carbon or 0.76 and 0.8 for gold, respectively. The dotted lines correspond to electrons with no energy loss.

ments. The energy spectra calculated for grain diameters 300 nm and above are (within the modeling noise) equal and very similar to those for planar samples. The only difference is a little large portion of higher energies (above 7 keV) scattered from the spherical samples. The scattered yield of 10 keV electrons is equal to unity for 100 nm gold grains [$D_l \approx 100$ nm, Fig. 4(a)] and thus the spectrum of the scattered electrons becomes harder and this hardening continues with the decreasing grain size. As it can be seen from the figure, no energies below 6.5 keV are present in the spectrum of electrons scattered from the 50 nm grain.

The modeled spectrum for carbon [Fig. 5(b)] is rather flat, again in a good agreement with measurements for light elements.[5] Comparing to the plate, the spectra of large spheres exhibit a larger portion of electrons with the energies close to the primary energy. Such effect was mentioned above for the gold samples but it is much more pronounced for carbon. The spectra grow at a whole energy range with a decreasing grain size up to ≈ 1 μm of grain diameter. For smaller grains, the spectrum shape changes because D_l of carbon is ≈ 600 nm. An underlaying area is equal to unity but low-energy electrons disappear and the energy corresponding to the maximum approaches the primary energy. The spectrum becomes harder because the number of collisions of the primary electrons needed to pass through a grain decreases.

The mean energy of scattered electrons is plotted in Fig. 6 as a function of the primary energy. The standard deviation for both gold and glassy carbon grains (not plotted) is $\approx 20\%$. At a full energy range, electrons leave 44% and 24% of their energy inside a glassy carbon and gold plates, respectively. This portion is smaller for large grains (36% and 20%, respectively) and does not change until η reaches unity. Then, the mean energy of scattered electrons gradually approaches the primary energy as losses inside small grains decrease. These effects are very important for interaction of dust clouds with energetic electrons. Let us consider a 10 keV electron flying into the cloud formed by 50 nm glassy carbon grains. The electron leaves about 50 eV inside first grain and continues to other grain until its energy drops to ≈ 1.5 keV and it can be caught inside some grain. On its path, the electron meets ≈ 50 grains and it excites ≈ 15 secondary electrons.

Finally, we would like to point out that the corrected model is 3D, can deal with grains of arbitrary shapes and can simulate the dust grains that consist of several material layers or small features embedded inside the grain. However, the spherical symmetry simplifies the calculations because the grain charging should be taken into account. It can be shown that the distribution of incidence angles conserves its shape for charged spheres but it is not true for an arbitrary form of the grain or its parts. We should point out that the scattered yield is a ratio of the number of primary electrons reaching the grain surface due to collisions with the grain atoms to the number of primary electrons. The fact that the electron reaches the surface does not necessarily mean that it will be emitted; it depends on its energy and the grain potential. Consequently, both the scattered yield (Fig. 2) and energetic spectrum of the scattered electrons (Fig. 5) should be considered for the grain charging. Moreover, the scattering of primary electrons inside the grain is accomplished with the generation of true secondary electrons and their yield can be rather large. Taken the 50 nm carbon grain and primary energy of 10 keV as an example, one can see that all primary electrons will be scattered to the surface [Fig. 2(a)] with the energy exceeding 8 keV [Fig. 3(a)]. All these electrons leave the grain if its potential will be lower than 8 kV and thus they do not contribute to the charging. In such a case, the grain potential is determined by the energy spectrum of secondary electrons and, as discussed in Pavlů *et al.*,[31] limited approximately to a half of the primary energy.

IV. CONCLUSION

The paper discusses the interaction of energetic electrons with solids and is focused on small bodies. The discussion resulted in several corrections of the model of the dust grain charging by Richterová *et al.*[1] Suggested corrections are

especially important for dust grains consisting of light species that can be frequently found in the space as well as in laboratory or industrial applications. The results of the corrected model are presented in several plots and they were successfully applied for interpretation of experimental investigations of the Mars dust simulant[32] or for calculations of the influence of the salt content in the icy dust grains on their charging properties.

ACKNOWLEDGMENTS

This work was supported in part by Research Plan No. MSM 0021620860 financed by the Ministry of Education of the Czech Republic, partly supported by the Czech Grant Agency under Contracts No. 202/08/P066, No. 202/08/0063, and No. 202/08/H057, and partly funded by the Grant Agency of Charles University (Grant No. GAUK 146207).

*jiri.pavlu@mff.cuni.cz

[1] I. Richterová, J. Pavlů, Z. Němeček, and J. Šafránková, Phys. Rev. B **74**, 235430 (2006).
[2] N. Meyer-Vernet, Astron. Astrophys. **105**, 98 (1982).
[3] U. de Angelis, Phys. Scr. **45**, 465 (1992).
[4] C. K. Goertz, Rev. Geophys. **27**, 271 (1989).
[5] I. M. Bronstein and B. S. Fraiman, *Secondary Electron Emission* (Nauka, Moskva, 1969) (in Russian).
[6] M. M. El Gomati, C. G. H. Walker, A. M. D. Assa'd, and M. Zadražil, Scanning **30**, 2 (2008).
[7] C. G. H. Walker, M. M. El Gomati, A. M. D. Assa'd, and M. Zadražil, Scanning **30**, 365 (2008).
[8] D. Drouin, P. Hovington, and R. Gauvin, Scanning **19**, 20 (1997).
[9] H. A. Bethe, *Handbook of Physics* (Springer, Berlin, 1933), Vol. 24.
[10] P. Hovington, D. Drouin, R. Gauvin, D. C. Joy, and N. Evans, Scanning **19**, 29 (1997).
[11] E. Rutherford, Philos. Mag. **21**, 669 (1911).
[12] D. C. Joy and S. Luo, Scanning **11**, 176 (1989).
[13] N. Mott and H. Massey, *Theory of Atomic Collisions* (Oxford University Press, New York, 1965).
[14] R. Browning, T. Z. Li, B. Chui, Y. Jun, R. F. W. Pease, Z. Czyzewski, and D. C. Joy, Scanning **17**, 250 (1995).
[15] Z. Czyżewski, D. O'Neill MacCallum, A. Romig, and D. C. Joy, J. Appl. Phys. **68**, 3066 (1990).
[16] B. Draine and E. Salpeter, Astrophys. J. **231**, 77 (1979).
[17] P. Ziemann, P. Liu, D. Kittelson, and P. McMurry, J. Phys. Chem. **99**, 5126 (1995).
[18] J. Švestka, I. Čermák, and E. Grün, Adv. Space Res. **13**, 199 (1993).
[19] J. Pavlů, I. Richterová, Z. Němeček, J. Šafránková, and I. Čermák, Faraday Discuss. **137**, 139 (2008).
[20] V. Chow, D. Mendis, and M. Rosenberg, IEEE Trans. Plasma Sci. **22**, 179 (1994).
[21] I. Richterová, Z. Němeček, J. Šafránková, and J. Pavlu, IEEE Trans. Plasma Sci. **32**, 617 (2004).
[22] I. Richterová, Z. Němeček, J. Šafránková, J. Pavlu, and M. Beránek, IEEE Trans. Plasma Sci. **35**, 286 (2007).
[23] P. Hovington, D. Drouin, and R. Gauvin, Scanning **19**, 1 (1997).
[24] M. J. Berger and S. M. Seltzer, U.S. Department of Commerce Report No. NBSIR 82-2550-A, 1984.
[25] D. C. Joy, S. Luo, R. Gauvin, P. Hovington, and N. Evans, Scanning Microsc. **10**, 653 (1996).
[26] H.-J. Hunger and L. Küchler, Phys. Status Solidi A **56**, K45 (1979).
[27] P. Palluel, Compt. Rend. **224**, 1492 (1947).
[28] E. J. Sternglass, Phys. Rev. **95**, 345 (1954).
[29] A. M. D. Assad and M. M. El Gomati, Scan. Electron Microsc. **12**, 185 (1998).
[30] Z. J. Ding, H. M. Li, K. Goto, Y. Z. Jiang, and R. Shimizu, J. Appl. Phys. **96**, 4598 (2004).
[31] J. Pavlů, J. Šafránková, Z. Němeček, and I. Richterová, Contrib. Plasma Phys. **49**, 169 (2009).
[32] M. Beránek, J. Pavlů, J. Vaverka, I. Richterová, J. Šafránková, and Z. Němeček (unpublished).